ChemComm

Accepted Manuscript

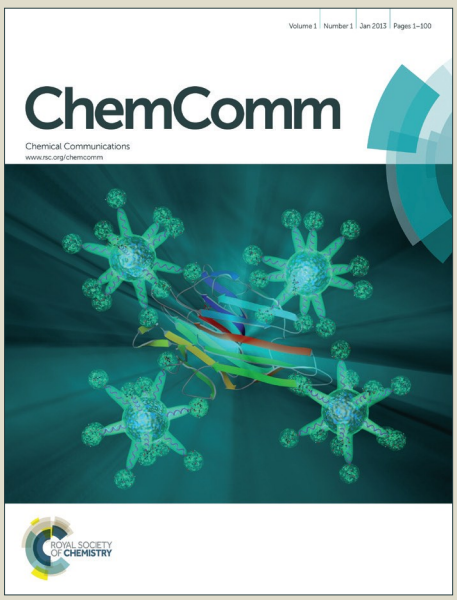

ROYAL SOCIETY OF CHEMISTRY

www.rsc.org/chemcomm

Journal Name

COMMUNICATION

Strong contribution of pore morphology to high-rate electrochemical performance of lithium-ion battery

Received 00th January 20xx,
Accepted 00th January 20xx

DOI: 10.1039/x0xx00000x

www.rsc.org/

Yeru Liang[a], Luyi Chen[a], Lifeng Cai[b], Hao Liu[a], Ruowen Fu[a], Mingqiu Zhang[a] and Dingcai Wu[a]*

The interconnected ordered pore channels facilitate faster permeation of Li^+ ions during charge-discharge process than the isolated ordered pore channels, resulting in significantly enhanced capacities, better rate capabilities and more remarkable cycling stability.

Lithium-ion batteries (LIBs) have been widely considered as a promising power source in many fields by virtue of their high energy density.[1] However, LIBs usually suffer from a low charge-discharge rate when compared with electrochemical capacitors.[2] With the ever-increasing and urgent energy storage demands for the applications in vehicle electrification devices, LIBs with both high energy capacity and power output are significantly desirable.[3] Therefore, improving the charge-discharge rate performance of LIBs without sacrificing their excellent energy storage properties is very valuable to the development of LIB devices.

In general, the power storage and the charge-discharge time of a LIB depend critically on the diffusion rate of Li^+ ions and electrons through the electrolyte and bulk electrodes into active sites.[2d, 4] In the past decades, many efforts have been devoted to increase ion and electron transport kinetics in batteries. Strategies have mainly focused on exploring of various new nanostructured electrode materials.[5] In particular, construction of a well-defined porous structure has been demonstrated to be the most efficient method for enhancing rate capability.[5b, 6]

Nevertheless, the fundamental understanding that how the porous structure affects LIBs performance is still in its early stages but very desirable for lithium ion storage. The main reason could be ascribed to the fact that the exact mechanism of ion transport within porous textures is very complex and thus it is limited to employ a targeted porous structure as the investigation model.[4b] One such limitation is that the uneven pore structure parameters (*i.e.*, surface area, pore tortuosity and pore size) influence the Li^+ ions diffusion and permeation paths in the electrode. Another limitation is that the large difference in framework structure including surface chemistry and crystallinity is very inadequate for modeling and characterizing the actual electrochemical reaction. These factors have severely impaired the elucidation of the precise correlation of the pore structure with the LIB performance, which is very unfavorable to their further application. Consequently, appropriate models of porous structure are highly required to show convincing direct evidence to clarify whether and how the pore structure affects the actual electrochemical properties of the active materials.

Herein we propose an interesting insight into the aforementioned important but neglected issue by designing proper well-defined porous model materials. As a model study, we focus on ordered mesoporous carbonaceous structure with different pore morphologies, considering the pore morphology is a vital structural factor that strongly determines the Li^+ ion transport pathways. As shown in Fig. 1a and 1d, we elaborately design and prepare two types of ordered mesoporous carbon (OMC) models, *i.e.*, OMC with channel-like pore (OMC-CP) and OMC with interconnected pore (OMC-IP). They have distinctly different pore morphologies: the former exhibits isolated and hexagonally arrayed channel-like mesopores among the continuous carbon framework, while the latter presents continuous mesopores between adjacent carbon nanorods which are isolated and hexagonally arrayed by carbon spacers. However, except for the pore morphology, OMC-CP and OMC-IP have similar grain morphology and pore parameters, including pore ordering, pore size, and surface area. Moreover, both of them present the same carbon framework structure including microcrystalline structure and surface chemistry, due to their identical carbon source and carbonization procedures. Therefore, OMC-CP and OMC-IP are very profitable to be adopted as perfect carbon models to clarify the correlation of the pore morphology with the LIB performance. It is found that

[a]*Materials Science Institute, PCFM Lab and GDHPPC Lab, School of Chemistry and Chemical Engineering, Sun Yat-sen University, Guangzhou 510275, P. R. China E-mail: wudc@mail.sysu.edu.cn*
[b]*College of Environmental and Biological Engineering, Putian University, Putian 351100, P. R. China*

† Electronic Supplementary Information (ESI) available: Experimental details and additional information about material characterization. See DOI: 10.1039/x0xx00000x

pore morphology has a strong contribution to the electrochemical properties of LIBs, especially for the rate performance. The interconnected ordered pore channels in OMC-IP facilitate facilitate faster permeation of Li^+ ions during charge-discharge process than the isolated pore channels in OMC-CP, leading to significantly enhanced capacities, better rate capabilities (*e.g.*, *ca.* 450 mAh/g at 12500 mA/g) and more remarkable cycling stability (*e.g.*, 1144 mAh/g after 600 cycles at 1000 mA/g) for OMC-IP.

As shown in Fig. S1, OMC-CP and OMC-IP were fabricated by hard-templating and soft-templating procedures, respectively. Fig. 2a depicts the low-angle XRD patterns of OMC-CP and OMC-IP. It can be seen that both samples possess three distinct Bragg diffraction peaks of the 2D hexagonal space group, (10), (11), and (20), indicating high periodic order arrangement of symmetry mesoporous structure.[7] The calculation from XRD measurements reflects the values of the unit cell parameters (*a*) of OMC-CP and OMC-IP are the same, *i.e.*, 11.1 nm. SEM images shown in Fig. S2 reveal that OMC-CP has a similar grain morphology to OMC-IP. TEM images of these two carbons in Fig. 1b and 1e present linear arrays of mesopores arranged in a regular pattern, further confirming their representative characteristics for the 2D hexagonal order mesoporous structure. However, viewed from the [001] direction, they have distinctly different pore morphologies. OMC-CP exhibits isolated and hexagonally arrayed channel-like mesopores among the continuous carbon framework (Fig. 1c). In contrast, OMC-IP is made up of hexagonally ordered arrays of carbon nanorods and presents continuous mesopores between adjacent carbon nanorods (Fig. 1f). That is to say, OMC-CP displays totally reverse pore morphology of the OMC-IP, as represented in Fig. 1a and 1d.

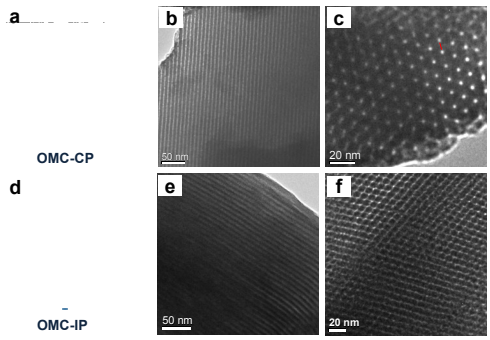

Fig. 1. Schematic diagram of (a) OMC-CP and (d) OMC-IP. TEM images of (b, c) OMC-CP and (e, f) OMC-IP, viewed from (b, e) the [110] and (c, f) the [001] directions.

The pore structures of OMC-CP and OMC-IP were further analyzed by N_2 adsorption measurement (Fig. S3). Both isotherms are type-IV with a distinct hysteretic loop at P/P_0 of 0.4~0.7, indicative of the porous nature with a uniformity of mesopore size.[8] As shown in the pore size distributions, both samples exhibit a unimodal pore size distribution (Fig. 2b). The pore diameter of OMC-IP (4.3 nm) is almost the same as that of OMC-CP (4.6 nm), and the thickness of carbon walls of OMC-IP and OMC-CP is 6.8 and 6.5 nm, respectively (Table S1). Furthermore, the BET surface area of OMC-IP is measured to be 1030 m^2/g, which is close to that of OMC-CP (896 m^2/g). These results clearly highlight that except for the pore morphology, OMC-CP and OMC-IP prepared here have very similar pore structure parameters.

Information about the difference of the carbon framework between OMC-CP and OMC-IP was determined by X-ray diffraction (XRD) pattern and Raman spectrum. Both OMC-CP and OMC-IP show very similar results, *i.e.*, broad peaks centered at $2\theta \approx 24^\circ$ and 43° in the XRD profiles, and characteristic peaks located at around 1340 cm^{-1} and 1600 cm (Fig. S4 and S5). The calculated interlayer spacing (d_{002}), stack height (L_c) and stack width (L_a) of OMC-IP are 0.371, 1.61 and 1.75 nm, respectively, which are almost consistent with that of OMC-CP (Tables S2~S3). These findings confirm that both OMC-CP and OMC-IP possess low graphite crystallinity of carbon framework. The chemical nature of the samples were analyzed by Fourier-transform infrared (FTIR) spectroscopy, X-ray photoelectron spectroscopy (XPS) and combustion elemental analysis. In the FTIR and XPS measurements, it is clear that OMC-CP and OMC-IP seem to have essentially similar infrared spectra (Fig. S6 and S7). Detailed XPS and combustion elemental analysis data demonstrate that carbon, oxygen and hydrogen contents in these two carbons are almost consistent (Table S4), indicating their chemical composition and surface chemistry are almost the same. It could be ascribed to their identical carbon source (*i.e.*, phenol/formaldehyde resin) and carbonization procedure.

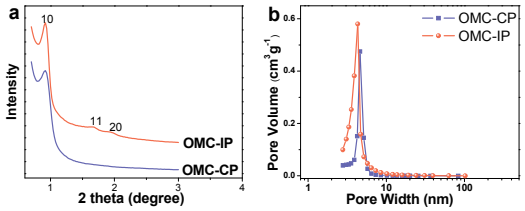

Fig. 2. (a) Low-angle XRD patterns and (b) pore size distributions of OMC-CP and OMC-IP.

The obtained OMC-CP and OMC-IP were used as a LIB anode under the same electrode-fabrication technique, and their electrochemical storage capacity was evaluated by using a standard half-cell configuration. Fig. S8 shows the first three charge-discharge curves at the current density of 100 mA/g between 0.01 and 3.0 V (*vs.* Li^+/Li). The first discharge capacity of OMC-CP (*i.e.*, 4101 mAh/g) is very close to that of OMC-IP (*i.e.*, 3934 mAh/g), which could be ascribed to their similar pore structure. Such high values considerably exceed the theoretical capacity of graphite (*i.e.*, 372 mAh/g).[9] This is a common phenomenon for non-graphitic carbons with high porosities.[6a, 10] It is suggested that in addition to the classical graphite intercalation mechanism, there exist other lithium storage mechanisms like lithium multi-layers on carbonaceous sheets, Li-C-H bond and metallic lithium clusters in microcavities for OMC-CP and OMC-IP.[10b, c, 11] The existence of these multiple lithium-storage positions in OMC-CP and OMC-IP gives rise to high capacities. In the second charge-discharge process, the discharge capacities of both OMC-CP and OMC-IP are decreased to 1328 and 2201 mAh/g, respectively. These

irreversible capacities could be attributed to the formation of solid electrolyte interface (SEI) layer at the surface of electrodes caused by reduction of the electrolyte, and to the irreversible electrochemical reactions caused by insertion of Li^+ ions into special positions in the ordered mesoporous carbon wall. In the subsequent electrochemical cycles, the capacities become more stable and reversible. Notably, OMC-IP possesses superior charge and discharge capacities to OMC-CP.

The cycling performance of OMC-CP and OMC-IP was evaluated at 100 and 1000 mA/g under the same configuration (Fig. S9). At the low current density of 100 mA/g, since the ions have enough time for diffusion throughout the nanopore systems and the subsequent insertion, the OMC-IP with higher surface area presents a little larger capacity (Fig. S9a). With increasing the current density to 1000 mA/g, the discharge capacities between OMC-CP and OMC-IP become significantly different (Fig. S9b). For the OMC-CP electrode, the reversible capacity sharply decrease to 517 mAh/g in the first cycle and then further decrease to 302 mAh/g after 600 cycles, giving a capacity retention ratio of 58% and a decrease of 0.07% per cycle. In sharp comparison, the discharge capacity increase to 1144 mAh/g after 600 cycles, exhibiting excellent stability with high capacity, especially at a high rate, *e.g.*, 1000 mA/g.

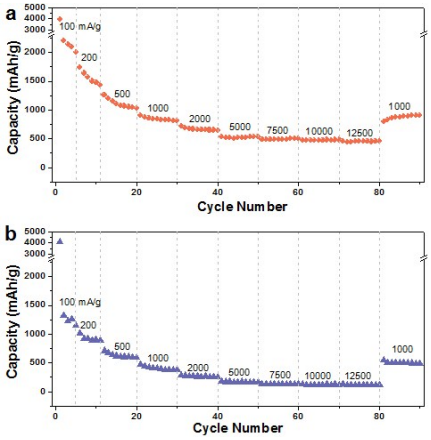

Fig. 3. Discharge capacity over cycling of (a) OMC-IP and (b) OMC-CP electrodes under different current densities varying from 100 to 12500 mA/g.

The difference of rate capability between OMC-CP and OMC-IP anodes was evaluated in detail at various current densities from 100 to 12500 mA/g. It can be found in Fig. 3 that OMC-IP exhibits much better rate performance than OMC-CP. For example, the discharge capacities of OMC-IP at the relatively low current density like 200 mA/g, are in the range of 1428~1737 mAh/g, which are higher than that of OMC-CP (887~1014 mAh/g). With raising the current density to 500~12500 mA/g, the difference in capacities between these two carbon electrodes becomes more and more distinct. In the case of OMC-CP electrode, the rate capacity drops sharply with increasing discharge rate. With an increase of the current density to 12500 mA/g, a small capacity of approximately 120 mAh/g is delivered by OMC-CP (Fig. 3b). On the other hand, the capacities for OMC-IP can be discharged up to about 1266 mAh/g at 500 mA/g. Even under the very high current density of 12500 mA/g, the capacity of OMC-IP electrode can unexpectedly retain a large value of *ca.* 45 mAh/g, which is still higher than the theoretical value of graphite. This value also exceeds that of many previously reported typical anode materials at high current densities (*e.g.* 12500 mA/g).[6c, 12] Furthermore, when the current density is tuned back to 1000 mA/g after cycling and cycling at different current densities (*i.e.*, 100~12500 mA/g), the capacity of OMC-IP can be recovered to about 900 mAh/g, demonstrating highly stable cycling performance (Fig. 3a). These results highlight that OMC-IP is more suitable to be an electrode that can tolerate ultrafast extraction/insertion of Li^+ ions at high rates.

Thus, the fundamental questions are: what is the key factor in determining the electrochemical properties and how does it affect the battery performance? It has been shown that many nanostructure parameters such as pore size, pore ordering, surface area, grain morphology and carbon framework could affect the Li^+ ion transportation in the nanopore system. However, as well revealed above, the as-prepared OMC-CP and OMC-IP electrodes have very similar nanostructure parameters including pore size, pore ordering, BET surface area, grain morphology, microcrystalline structure, thickness of carbon wall and surface chemistry. All these factors except for the pore morphology are eliminated during gaining insights into the effects of structural parameters on electrochemical performance. Therefore, it is believed that the superior high-rate performance in OMC-IP is convincingly due to its advanced pore morphology. For the OMC-CP, the ordered pore channels are isolated by the carbon walls; therefore, the Li^+ ions permeate into the carbon wall only through its adjacent limited pore channels (Fig. 4a). In contrast, the OMC-IP is constructed with an ordered array of carbon nanorods and can provide a larger void space for dispersion of Li^+ ions. In such an interconnected pore system, the Li^+ ions can easily and rapidly permeate into the carbon wall from various surrounding directions. As a result, the fast ion diffusion behavior in OMC-IP is more excellent due to its more ion permeation routes, leading to better capacity retention.

On the other hand, a significant difference in capacity is observed between OMC-CP and OMC-IP, particularly at the high charge-discharge rates (Fig. S9b). To verify the limiting factor accountable for this difference, electrochemical impedance spectroscopy measurement of these two carbon electrodes is performed, and the obtained Nyquist complex plane impedance plots are displayed in Fig. 4b. Meanwhile, the impendence spectra are modelled by the modified equivalent circuit (Fig. S10). Two semicircle arcs in the high- and medium-frequency regions and a linear line in the low frequency range can be observed for both electrodes. The high-frequency arc is associated with the resistance (R_f) and constant phase element (CPE_1) of the SEI film.[4d, 13] It can be seen that the arc diameter of OMC-IP is smaller than that of OMC-CP in this region, indicating that OMC-IP can promote the penetration of electrolytes into the SEI film more effectively than OMC-CP. The medium frequency region is ascribed to the charge-transfer impedance (R_{ct}) and CPE_2 on electrode/electrolyte

interface. As illustrated in Fig. 4b, OMC-IP possesses a smaller charge-transfer resistance relative to OMC-CP, indicative of a lower ionic resistance and superior kinetics for OMC-IP. This is a result of its interconnected pore structure which can offer large electrode/electrolyte interface for the charge-transfer reaction. Overall, the pore morphology of porous carbons plays a decisive factor in determining electrochemical properties of LIB, especially at high rates.

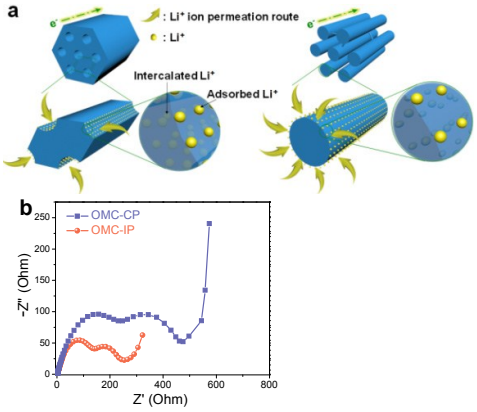

Fig. 4. (a) Schematic representation of electron transport, Li^+ ion storage and Li^+ ion penetration routes; (b) Nyquist impedance plots of OMC-CP and OMC-IP electrodes.

In summary, we provide a convincing direct evidence to demonstrate that there is a strong contribution of pore morphology to the electrochemical performances of LIB. This is based on design, fabrication and electrochemical characterization of two classes of perfect carbon models, *i.e.*, OMC-CP and OMC-IP, which possess the identical carbon framework and very similar pore structure except for the pore morphology. It was demonstrated that the interconnected ordered pore channels in OMC-IP facilitate faster permeation of Li^+ ions during charge-discharge process than the isolated ordered pore channels in OMC-CP, resulting in significantly enhanced capacities, better rate capabilities and more remarkable cycling stability for OMC-IP. Our results show the fundamental understanding about how the porous morphology affects the dynamic processes of the guest species like Li^+ ions. We anticipate that such a work would be useful in the development of high-performance energy devices by exploiting the properties of rational nanostructures that allow for fast mass transfer.

This work was supported by the projects of the National Natural Science Foundation of China (51422307, 51372280, 51173213, 51172290 and 51232005), China Postdoctoral Science Foundation (2014M560686, 2015T80932), Guangdong Natural Science Funds for Distinguished Young Scholar (S2013050014408), Program for New Century Excellent Talents in University by Ministry of Education (NCET-12-0572), Pearl River S&T Nova Program of Guangzhou (2013J2200015), Fundamental Research Funds for the Central Universities (15lgjc17, 13lgpy57) and National Key Basic Research Program of China (2014CB932400).

References

1. (a)J. M. Tarascon and M. Armand, *Nature*, 2001, **414**, 359; (b)D. Su and R. Schlogl, *Chemsuschem*, 2010, **3**, 136; (c)Y. Su, Y. Liu, P. Liu, D. Wu, X. Zhuang, F. Zhang and X. Feng, *Angew. Chem. Int. Ed.* , 2015, **54**, 1812; (d)M. S. Whittingham, *Chem. Rev.* , 2004, **104**, 4271; (e)J. B. Goodenough and K.-S. Park, *J. Am. Chem. Soc.* , 2013, **135**, 1167.
2. (a)B. Kang and G. Ceder, *Nature*, 2009, **458**, 190; (b)W. F. Zhang, Z. H. Huang, G. P. Cao, F. Y. Kang and Y. S. Yang, *J. Power Sources* 2012, **204**, 230; (c)M. Armand and J. M. Tarascon, *Nature*, 2008, **451**, 652; (d)N. Li, Z. P. Chen, W. C. Ren, F. Li and H. M. Cheng, *PNAS* 2012, **109**, 17360.
3. (a)B. Dunn, H. Kamath and J.-M. Tarascon, *Science*, 2011, **334**, 928; (b)C. Liu, F. Li, L. P. Ma and H. M. Cheng, *Adv. Mater.* , 2010, **22**, E28; (c)D. M. Piper, T. Evans, K. Leung, T. Watkins, J. Olson, S. C. Kim, S. S. Han, V. Bhat, K. H. Oh, D. A. Buttry and S.-H. Lee, *Nat. Commun.*, 2015, **6**.
4. (a)M. T. McDowell, S. W. Lee, W. D. Nix and Y. Cui, *Adv. Mater.* , 2013, **25**, 4966; (b)K. J. Lee, W. Bak, J. J. Kim, M. A. Snyder, W. C. Yoo and Y. E. Sung, *J. Phys. Chem. C* 2015, **119**, 7604; (c)Y. W. Zheng, S. Cui, X. Song, Y. Su, W. Deng, Z. Wu, X. Wang, W. Wang, M. Rao, Y. Lin, C. Wang, K. Amine and F. Pan, *J. Am. Chem. Soc.* 2015, **137**, 8364; (d)Y. Tang, Y. Zhang, J. Deng, D. Qi, W. R. Leow, J. Wei, S. Yin, Z. Dong, R. Yazami, Z. Chen and X. Chen, *Angewandte Chemie*, 2014, **126**, 13706.
5. (a)J. Qin, W. Lv, Z. Li, B. Li, F. Kang and Q.-H. Yang, *Chem. Commun.* , 2014, **50**, 13447; (b)H. G. Zhang, X. D. Yu and P. Braun, *Nat. Nanotechnol.* , 2011, **6**, 277; (c)Z. S. Wu, L. L. Xue, W. C. Ren, F. Li, L. Wen and H. M. Cheng, *Adv. Funct. Mater.* , 2012, **22**, 3290; (d)D. Kong, H. He, Q. Song, B. Wang, W. Lv, Q.-H. Yang and L. Zhi, *Energy Environ. Sci.* , 2014, **7**, 3320; (e)Y. Tang, Y. Zhang, W. Li, B. Ma and X. Chen, *Chem. Soc. Rev.* , 2015.
6. (a)L. Qie, W. M. Chen, Z. H. Wang, Q. G. Shao, X. Li, L. X. Yuan, X. L. Hu, W. X. Zhang and Y. H. Huang, *Adv. Mater.* , 2012, **24**, 2047; (b)Y. R. Liang, L. F. Cai, L. Y. Chen, X. D. Lin, R. W. Fu, M. Q. Zhang and D. C. Wu, *Nanoscale*, 2015, **7**, 3971; (c)J. Wang, N. Yang, H. Tang, Z. Dong, Q. Jin, M. Yang, D. Kisailus, H. Zhao, Z. Tang and D. Wang, *Angew. Chem. Int. Ed.* , 2013, **52**, 6417.
7. (a)Y. Meng, D. Gu, F. Zhang, Y. Shi, L. Cheng, D. Feng, Z. Wu, Z. Chen, Y. Wan, A. Stein and D. Zhao, *Chem. Mater.* , 2006, **18**, 4447; (b)S. Jun, S. H. Joo, R. Ryoo, M. Kruk, M. Jaroniec, Z. Liu, T. Ohsuna and O. Terasaki, *J. Am. Chem. Soc.* , 2000, **122**, 10712.
8. (a)S. Li, Y. Liang, D. Wu and R. Fu, *Carbon*, 2010, **48**, 839; (b)F. Xu, G. Zheng, D. Wu, Y. Liang, Z. Li and R. Fu, *PCCP* 2010, **12**, 3270.
9. F. Zheng, Y. Yang and Q. Chen, *Nat. Commun.*, 2014, **5**.
10. (a)H. S. Zhou, S. M. Zhu, M. Hibino, I. Honma and M. Ichihara, *Adv. Mater.* , 2003, **15**, 2107; (b)N. A. Kaskhedikar and J. Maier, *Adv. Mater.* , 2009, **21**, 2664; (c)S. Yang, X. Feng, L. Zhi, Q. Cao, J. Maier and K. Müllen, *Adv. Mater.* , 2010, **22**, 838.
11. I. Mochida, C.-H. Ku, S.-H. Yoon and Y. Korai, *J. Power Sources* 1998, **75**, 214.
12. (a)X. Yang, H. Huang, Z. Li, M. Zhong, G. Zhang and D. Wu, *Carbon*, 2014, **77**, 275; (b)H. Liu, Z. Li, Y. Liang, R. Fu and D. Wu, *Carbon*, 2015, **84**, 419; (c)F.-H. Du, B. Li, W. Fu, Y.-J. Xiong, K.-X. Wang and J.-S. Chen, *Adv. Mater.* , 2014, **26**, 6145; (d)X. Zhou, J. Dai, S. Liu, J. Bao and Y.-G. Guo, *Adv. Mater.* , 2014, **26**, 3943; (e)G. Chen, Z. Wang and D. Xia, *Chem. Mater.* , 2008, **20**, 6951.
13. Y. Zhang, T. Chen, J. Wang, G. Min, L. Pan, Z. Song, Z. Sun, W. Zhou and J. Zhang, *Appl. Surf. Sci.* , 2012, **258**, 4729.